Electronic Supplementary Material (ESI) for Chemical Communications.

Pomegranate-Like Multicore-Shell Mn_3O_4 Encapsulated Mesoporous N-Doped Carbon with Internal Void Space for High-Performance Lithium-Ion Batteries

Yingwei Liu, Jie Han, Lei Fan, Yanan Li, Rong Guo**

School of Chemistry and Chemical Engineering, Yangzhou University, Yangzhou, Jiangsu, 225002, P. R. China. E-mail: hanjie@yzu.edu.cn; guorong@yzu.edu.cn

Experimental Section

Materials

Aniline was distilled under reduced pressure before use. Colloidal silica (SiO_2, 40 wt%) was obtained from Sigma-Aldrich. $KMnO_4$ (≥99.5 %) and other reagents were purchased from Sinopharm Chemical Agent, Co. Ltd, which were of analytical grade and used as received without further purification. The deionized water (18.2 MΩ) used in this study was taken from Barnstead LabTower EDI ultrapure water system (Thermo Scientific, USA).

Preparation of m-N-C nanospheres

m-N-C nanospheres was prepared according to the reference with modification.[1] In a typical reaction, 1 mL SiO_2 colloidal aqueous solution, 5 mL HCl aqueous solution (1 mol/L) and 0.4 mL aniline monomer were dispersed into 10 ml deionized water by sonication. Then, ammonium persulphate aqueous solution (1 g ammonium persulphate dissolved in 2 mL 1 mol/L HCl aqueous solution) was dropped into the above suspension to initiate the polymerization of aniline monomer under vigorous stirring in an ice bath, and the reaction was kept for 24 h. The generated precipitates containing polyaniline and SiO_2 were centrifuged and washed with water and ethanol several times, and then dried at 60 ^oC for 12 h. After that, the products were annealed at 900 ^oC in N_2 to realize the carbonization of polyaniline, followed by sodium hydroxide treatment to remove SiO_2 template. Finally, m-N-C nanospheres with nanocavities were obtained.

Preparation of m-N-C@Mn_3O_4 nanopomegranates

In a typical synthesis, 10 mg m-N-C nanospheres and 10 mg $KMnO_4$ were added into 20 mL deionized water and the colloidal solution was sonicated to form a homogeneous suspension. Then, the suspension was transformed into a 45 mL Teflon-lined stainless steel autoclave and kept at 140 ^oC for 1 h. When the hydrothermal reaction was finished, the precipitates were centrifuged, washed with water several times, and then dried at 60 ^oC for 12 h. Finally, the products were annealed at 300 ^oC in N_2 for 2 h, resulting in the formation of m-N-C@Mn_3O_4 nanopomegranates.

Characterization

The SEM images were obtained on a field-emission scanning electron microscopy (FFSEM, Zeiss_Supra55, Germany). The TEM images were obtained on a transmission electron microscope (TEM, JEM-2100, Japan). HRTEM and HAADF-STEM images were taken on a field-emission transmission electron microscopoy (FETEM, Tecnai G2 F30 S-TWIN, Holland). XPS measurements were performed on a Thermo ESCALAB 250Xi photoelectron spectrometer (USA) using an Al Kα (1486.6 eV) gun as the excitation source and choosing C 1s as the reference line. XRD patterns were collected on a D8 Advanced X-ray diffractometer (Bruker, Germany). The products were recorded in the 2θ range from 10° to 80° in steps of 0.04° with a count time of 1 s each time. The specific surface area and pore size were studied by using a Beishide 3H-2000PS2 analysis instrument.

Electrochemical measurement

Anode electrodes were prepared according to the following procedures: the active materials (80 wt%), conductive carbon black (10 wt%, Super-P), and poly(vinylidene fluoride) binder (10 wt%) were dispersed into N-methylpyrrolidone to form a homogenous slurry. Then, the obtained slurry was pasted on Cu foil and the Cu foil was dried in a vacuum oven for 12 h at 80 ^{o}C to remove the solvent. The mass loading of the active material on the electrodes was about 1.0 mg cm^{-2}. After the electrode disks were cut to 1.6 cm diameter, the coin-type cell (CR2032) were assembled using the active materials' anode as the working electrode, the Li foil as the reference electrode and counter electrode, a Celgard 2325 as the separator, and 1 M lithium hexafluorophosphate ($LiPF_6$) in cosolvent of ethylene carbonate/dimethyl carbonate/ethyl methyl carbonate (EC/DEC/EMC, 1:1:1 by volume) as the electrolyte in a high-purity argon-filled glovebox (Vacuum Atmospheres Co., Ltd.). A VMP3 electrochemical workstation (Bio-logic, France) was not only used to measure electrochemical impedance spectra but also cyclic voltammetry curves in rage of 0.005~3 V at rate of 0.2 mV/s.

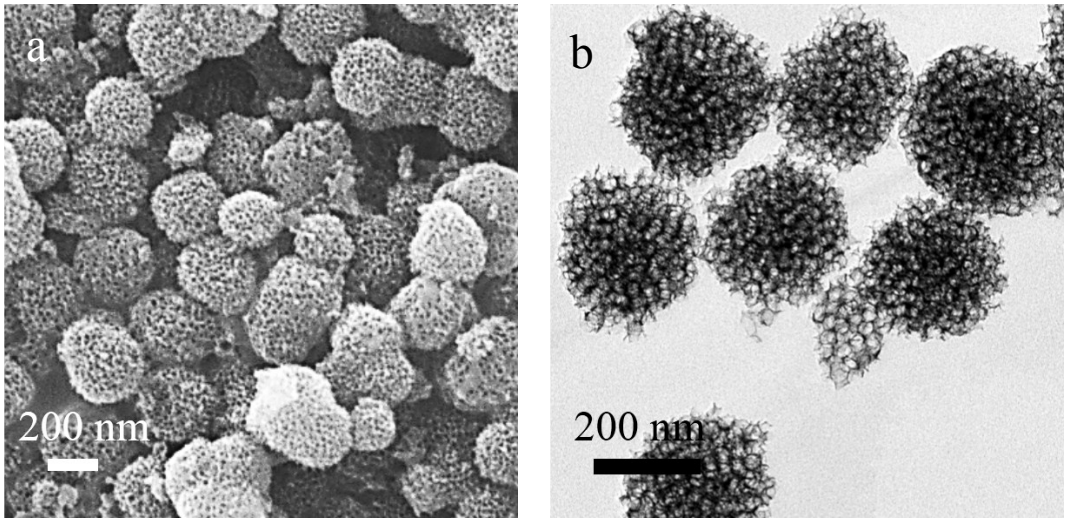

Figure S1. (a) SEM and (b) TEM images of m-N-C nanospheres.

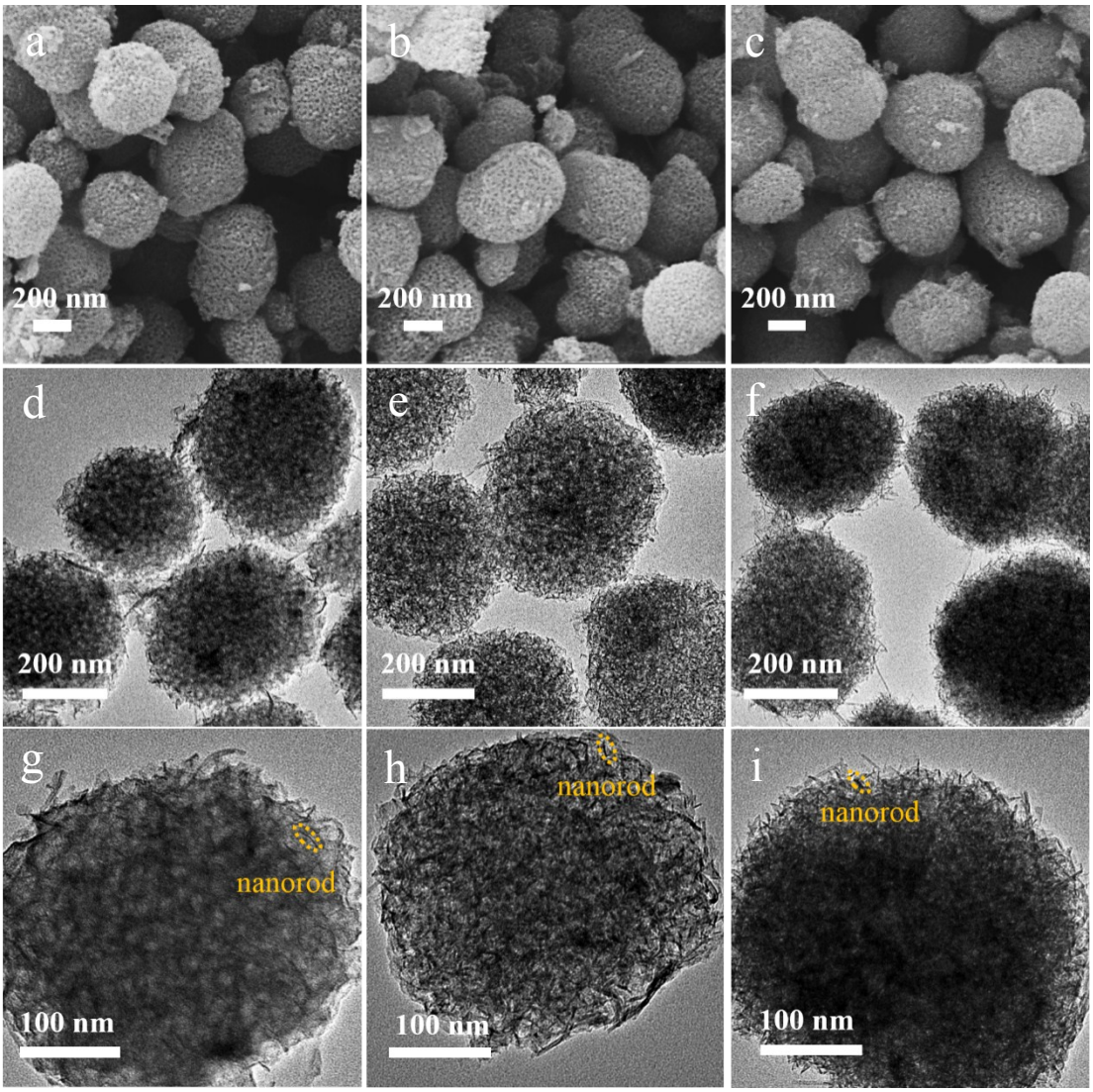

Figure S2. (a-c) SEM and (d-i) TEM images of m-N-C@MnO_2 synthesized at different amount of $KMnO_4$ (mg): (a, d, g) 5, (b, e, h) 10, and (c, f, i) 20.

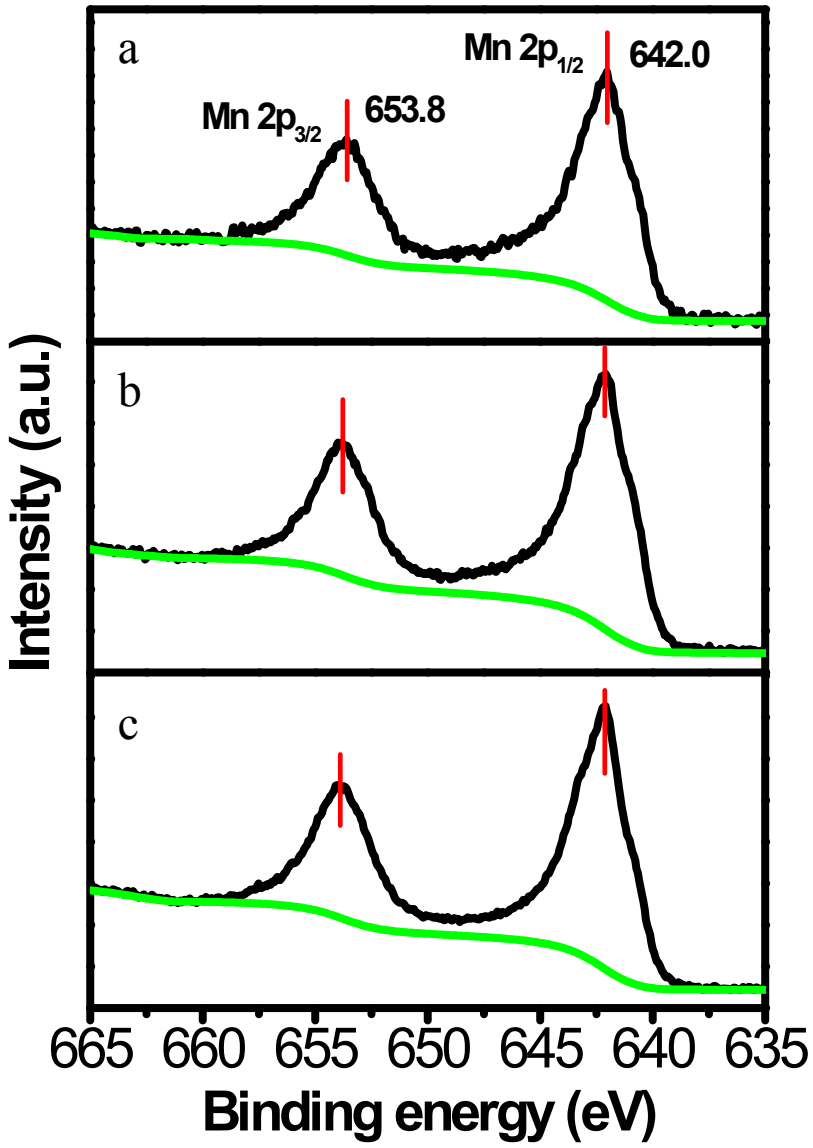

Figure S3. High-resolution Mn 2p spectra of m-N-C@MnO_2 synthesized at different amount of $KMnO_4$ (mg): (a) 5, (b) 10, and (c) 20.

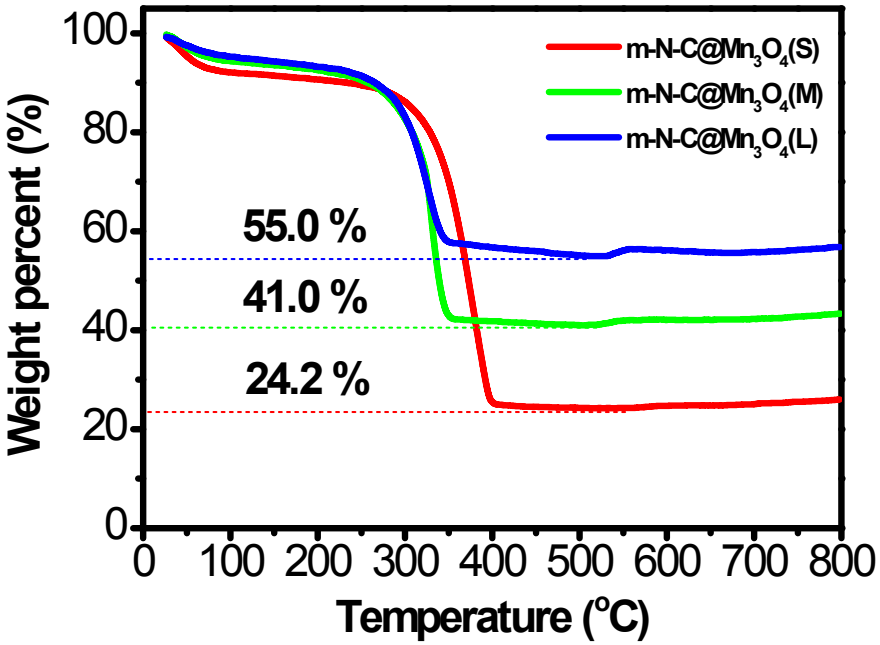

Figure S4. TGA curves of different samples under air atmosphere heated from room temperature to 800 °C with a ramping rate of 10 °C min^{-1}.

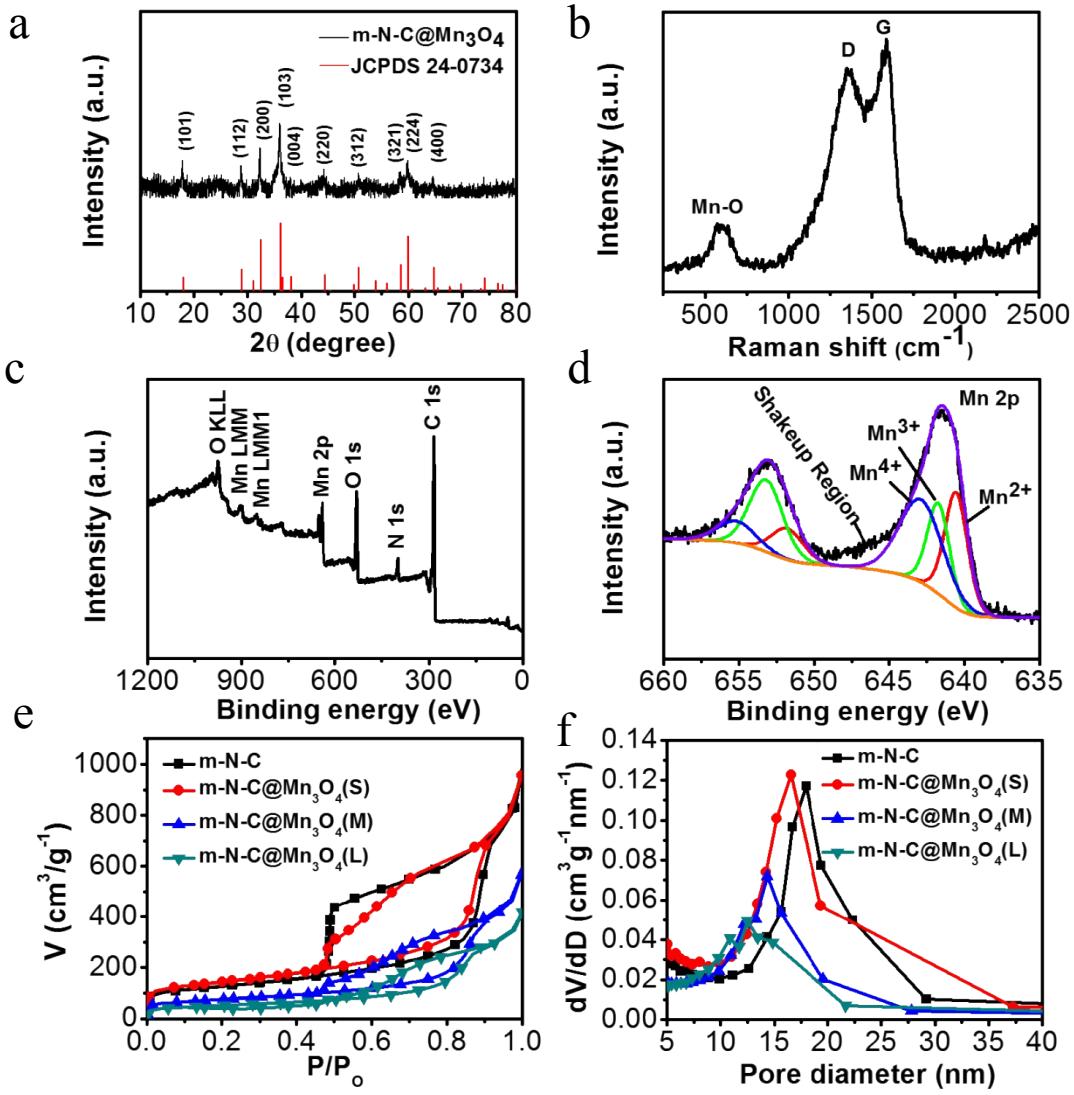

Figure S5. (a) XRD pattern, (b) Raman spectroscopy, (c) survey XPS spectrum, (d) high-resolution Mn 2p spectrum of m-N-C@Mn_3O_4(M) nanopomegranates. (e) N_2 absorption-desorption isotherms and (f) the corresponding pore size distributions of m-N-C and m-N-C@Mn_3O_4 nanopomegranates.

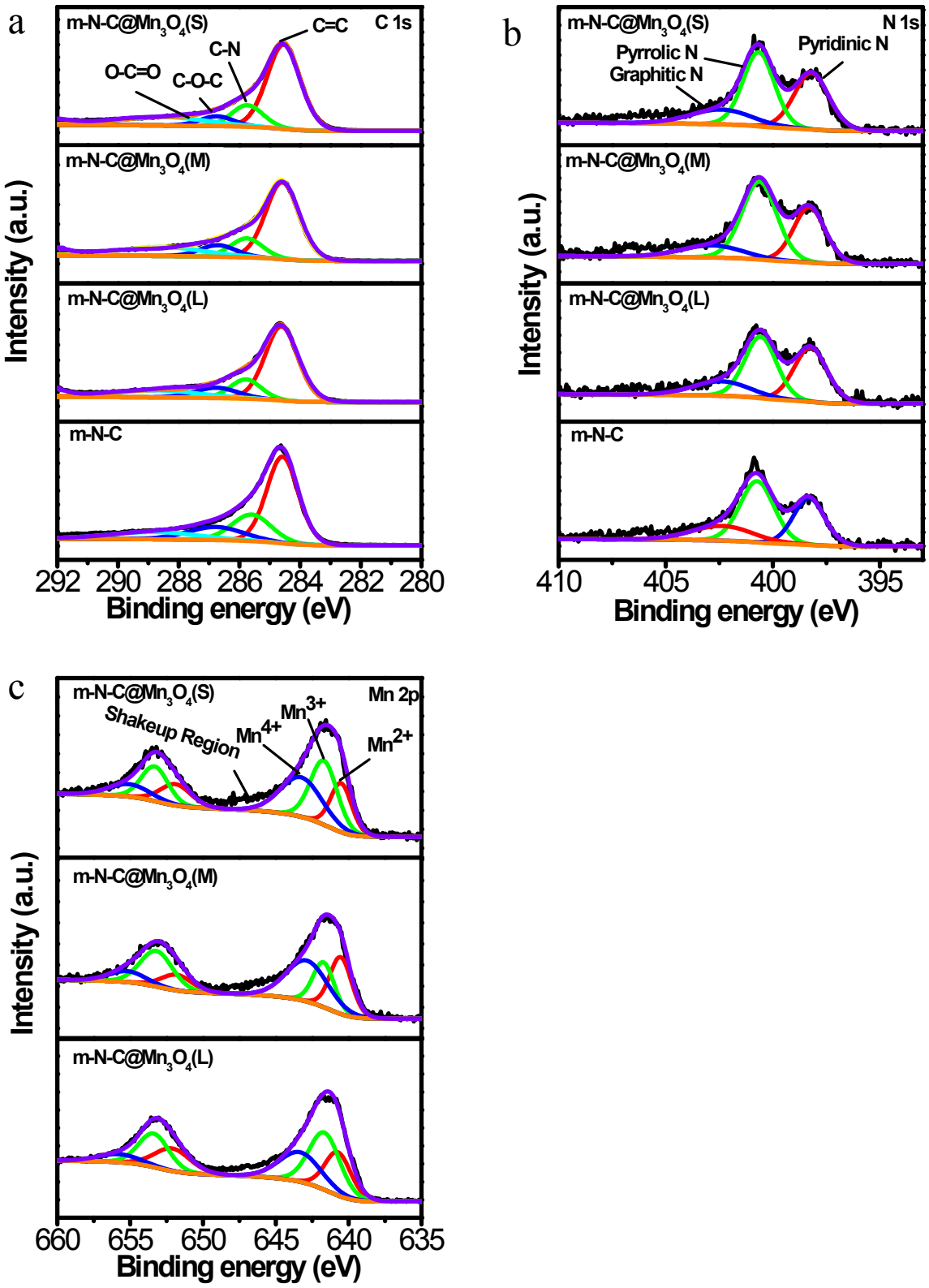

Figure S6. (a) High-resolution C 1s, (b) high-resolution N 1s and (c) high-resolution Mn 2p spectra of different samples.

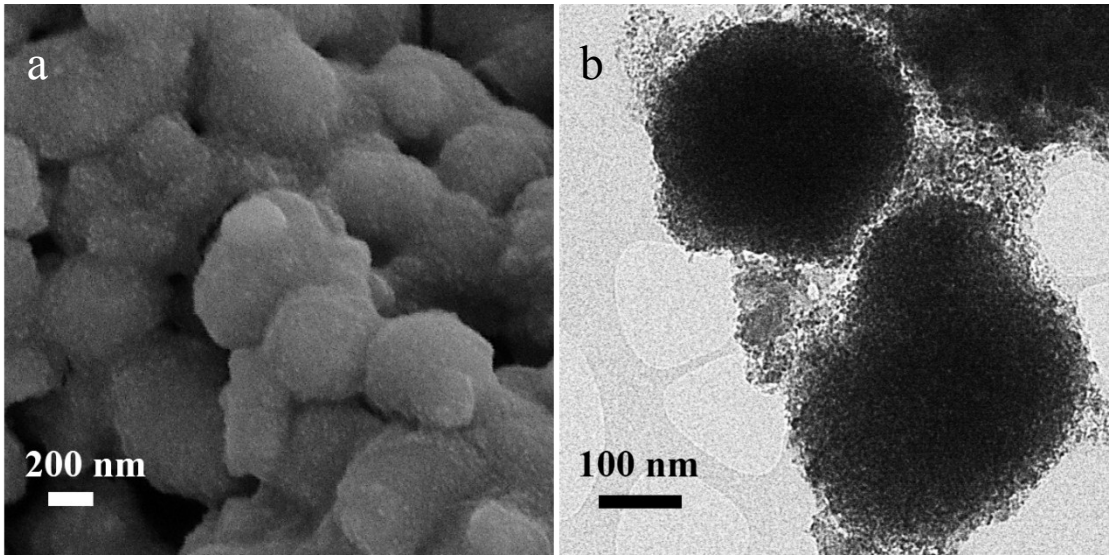

Figure S7. (a) SEM and (b) TEM images of m-N-C@Mn_3O_4(M) nanopomegranates after 800 cycles.

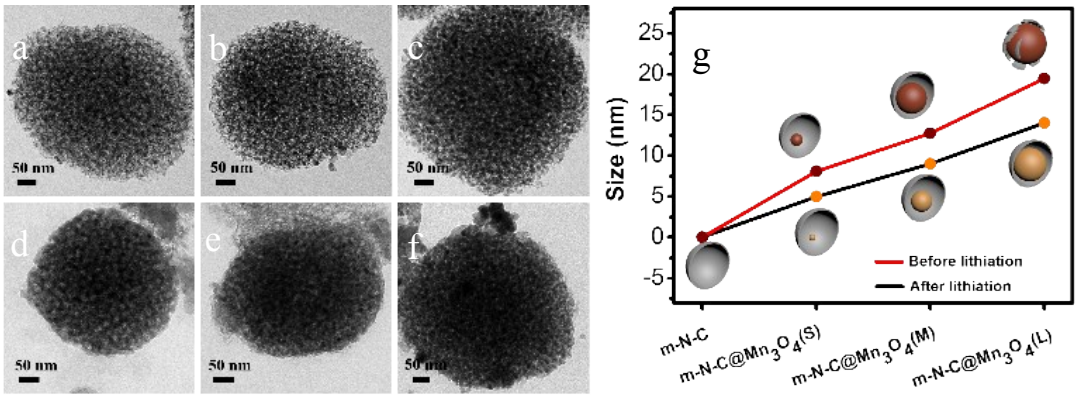

Figure S8. TEM images of (a) m-N-C@Mn_3O_4(S), (b) m-N-C@Mn_3O_4(M) and (c) m-N-C@Mn_3O_4(L) nanopomegranates before lithiation. TEM images of (d) m-N-C@Mn_3O_4(S), (e) m-N-C@Mn_3O_4(M) and (f) m-N-C@Mn_3O_4(L) nanopomegranates after lithiation. (g) The average size of Mn_3O_4 nanoparticles in m-N-C@Mn_3O_4 nanopomegranates before and after lithiation.

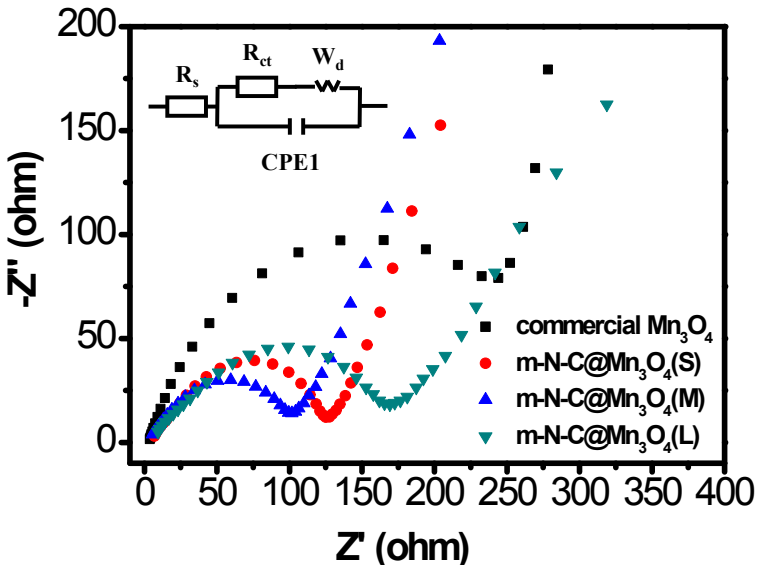

Figure S9. Niquist plots of commercial Mn_3O_4 and m-N-C@Mn_3O_4 nanopomegranates. Inset shows the equivalent circuit model.

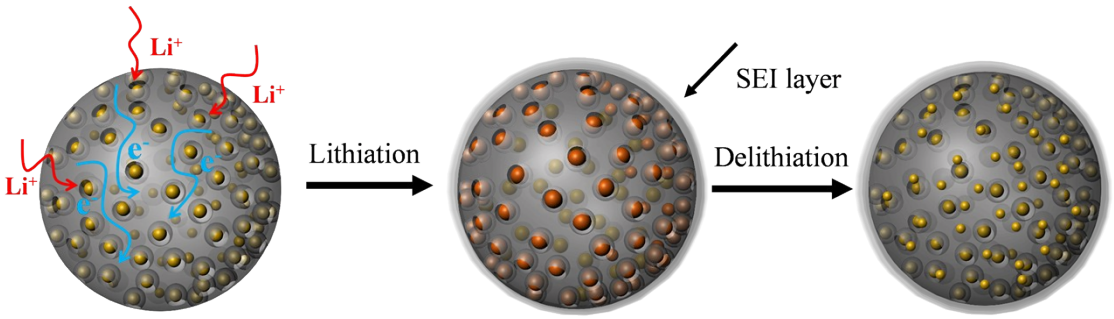

Figure S10. Schematic illustration of m-N-C@Mn_3O_4 nanopomegranates during lithiation and delithiation processes.

Table S1. Surface area and pore parameters of different samples.

Sample	Surface area ($m^2\ g^{-1}$)	Pore volume ($cm^3\ g^{-1}$)	Pore size (nm)
m-N-C	434.17	1.36	17.32
m-N-C@Mn_3O_4(S)	500.08	1.48	15.68
m-N-C@Mn_3O_4(M)	261.62	0.90	13.65
m-N-C@Mn_3O_4(L)	177.28	0.64	11.97

Table S2. EIS simulation results of commercial Mn_3O_4 and m-N-C@Mn_3O_4.

Sample	R_s (Ω)	R_{ct} (Ω)
commercial Mn_3O_4	3.53	184.40
m-N-C@Mn_3O_4(S)	5.43	119.60
m-N-C@Mn_3O_4(M)	3.65	92.06
m-N-C@Mn_3O_4(L)	5.52	172.00

Table S3. Performance comparison in this work with other preciously-reported Mn_3O_4-based materials for lithium-ion batteries.

Sample	Current density (mA g^{-1})	Cycle number	Capacity (mAh g^{-1})	Ref.
m-N-C@Mn_3O_4	1000	770	751	this work
Mn_3O_4 nano- octahedral	50	50	500	2
Mn_3O_4 micro/nanocuboids	1000	-	652	3
Mn_3O_4/grapheme composite	60	40	500	4
Graphene/ Mn_3O_4 nanocomposite membrance	100	100	702	5
Mn_3O_4-graphene hybrid	400	40	730	6
Mn_3O_4/carbon fiber hybrid	1000	-	552	7
Mn_3O_4 nanoparticles on hollow carbon fiber	1000	240	652	8
Mn_3O_4@C nanotube arrays	793	80	420	9
Urchin-like Mn_3O_4/carbon microspheres	1000	-	510	10
Acid-treated reduced graphene oxide/Mn_3O_4 nanorod nanocomposite	1000	-	509	11
Nanostructured Mn_3O_4/C Electrode	528	-	307	12
Ti^{3+} doped TiO_2 coated Mn_3O_4 nanorods	100	150	1488	13
3D Porous Mn_3O_4/G Composites	50	-	1425	14
Mn_3O_4/3D-graphene	1000	-	490	15

References

1 G. Wang, Y. Sun, D. Li, H.-W. Liang, R. Dong, X. Feng and K. Müllen, *Angew. Chem. Int. Ed.*, 2015, **54**, 15191-15196.

2 S. Z. Huang, J. Jin, Y. Cai, Y. Li, H. Y. Tan, H. E. Wang, G. Van Tendeloo and B. L. Su, *Nanoscale*, 2014, **6**, 6819-6827.

3 Y. Jiang, J. L. Yue, Q. B. Guo, Q. Y. Xia, C. Zhou, T. Feng, J. Xu and H. Xia, *Small*, 2018, **14**, 1704296.

4 I. Nam, N. D. Kim, G.-P. Kim, J. Park and J. Yi, *J. Power Sources*, 2013, **244**, 56-64.

5 J. G. Wang, D. Jin, R. Zhou, X. Li, X. R. Liu, C. Shen, K. Xie, B. Li, F. Kang and B. Wei, *ACS Nano*, 2016, **10**, 6227-6234.

6 H. L. Wang, L.-F. Cui, Y. Yang, H. S. Casalongue, J. T. Robinson, Y. Y. Liang, Y. Cui, and H. J. Dai, *J. Am. Chem. Soc.*, 2010, **132**, 13978-13980.

7 Z. Li and B. H. J. Tang, *Green Chem*., 2017, **19**, 5862-5873.

8 D. Zhang, G. Li, J. Fan, B. Li and L. Li, *Chem. Eur. J.*, 2018, **24**, 9632-9638.

9 B. Lu, J. Liu, R. Z. Hu, H. Wang, J. W. Liu and M. Zhu, *J. Mater. Chem. A*, 2017, **5**, 8555-8565.

10 S. Z. Huang, Y. Cai, J. Jin, J. Liu, Y. Li, Y. Yu, H. E. Wang and L. H. Chen, B. L. Su, *Nano Energy*, 2015, **12**, 833-844.

11 C. Y. Seong, S. K. Park, Y. Bae, S. Yoo and Y. Piao, *RSC Adv.*, 2017, **7**, 37502-37507.

12 M. H. Alfaruqi, J. Gim, S. Kim, J. Song, P. T. Duong, J. Jo, J. P. Baboo, Z. Xiu, V. Mathew and J. Kim, *Chem. Eur. J.*,2016, **22**, 2039-2045.

13 M. Y. Wang, Y. Huang, N. Zhang, Y. D. Zhu, H. M. Zhang and J.-K. Kim, *Chem. Eng. J.*, 2019, **370**, 1425-1433.

14 S. Li, L. L. Yu, Y.-T. Shi, J. Fan, R.-B. Li, G.-D.Fan, W.-L. Xu, and J.-T. Zhao, *ACS Appl. Mater. Interfaces,* 2019, **11**, 10178-10188.

15 C. Liu, Q.-Q. Ren, S.-W. Zhang, B.-S. Yin, L.-F. Que, L. Zhao, X.-L. Sui, F.-D. Yu, X. F. Li, D.-M. Gu, and Z.-B. Wang, *Chem. Eng. J.*, 2019, **370**, 1485-1492.